ACS Sustainable Chemistry & Engineering

Research Article

pubs.acs.org/journal/ascecg

# Oxygen Electroreduction Catalyzed by Palladium Nanoparticles Supported on Nitrogen-Doped Graphene Quantum Dots: Impacts of Nitrogen Dopants

Christopher P. Deming,[†] Rene Mercado,[†] Jia En Lu,[†] Vamsi Gadiraju,[‡] Mohammad Khan,[†] and Shaowei Chen*[,†]

[†]Department of Chemistry and Biochemistry, University of California, 1156 High Street, Santa Cruz, California 95064, United States

[‡]The Harker School, 4300 Bucknell Road, San Jose, California 95130, United States

Supporting Information

**ABSTRACT:** Palladium nanoparticles supported on nitrogen-doped graphene quantum dots (NGQD) were synthesized by hydrothermal coreduction of palladium salts, citric acid, and urea at 160 °C for up to 12 h. Transmission electron microscopic studies showed that in the resulting PdNGQD nanocomposites, small palladium nanoparticles clustered into superstructures of 100 nm and larger. X-ray photoelectron spectroscopic studies showed that the NGQDs contained only p-type pyridinic and pyrrolic nitrogen centers, and although the total concentrations of nitrogen dopants were rather consistent (ca. 10 at. %) among the series of samples, the relative abundance of pyrrolic (pyridinic) nitrogens increased (decreased) with prolonging reaction duration, suggesting thermal conversion of pyridinic nitrogens into pyrrolic ones. The binding energy of the Pd 3d electrons was found to increase accordingly, probably due to enhanced electron withdrawing by the more acidic pyrrolic nitrogens. This suggests apparent interactions between palladium and the nitrogen dopants. Consistent results were obtained in Raman spectroscopic measurements which showed an increase of the D and G band intensity ratio, indicative of an increasingly defective structure of the NGQD. This was consistent with the increasing abundance of pyrrolic centers which provided more structural strains than the six-membered pyridinic heterocycles within the graphitic backbone. Electrochemically, the series of PdNGQDs all showed apparent electrocatalytic activity toward oxygen reduction in alkaline media, and within the context of onset potential and kinetic current density, the sample prepared by 8 h of hydrothermal reaction was found to stand out as the best catalyst among the series, with a top specific activity that was over eight times better than that observed when palladium nanoparticles were supported on undoped GQDs and commercial Pt/C. This might be accounted for by the enhanced electron withdrawing effects of the pyrrolic nitrogen centers that manipulated the electronic interactions between palladium and oxygen intermediates, as compared to oxygenated moieties alone in undoped GQDs.

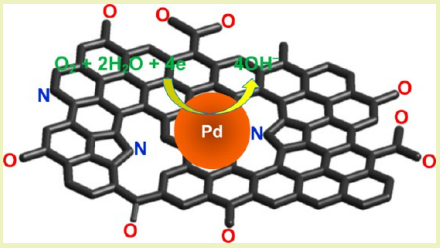


**KEYWORDS:** *Palladium nanoparticle, Nitrogen-doped, Graphene quantum dot, Defect, Hydrothermal, Oxygen reduction*

## INTRODUCTION

The advancement of fuel cells, in particular proton exchange membrane fuel cells, has been the focus of much research as it represents a promising route of clean renewable energy for mobile as well as stationary applications.[1−3] Currently, much research has been focused on the development of effective electrocatalysts, in particular, for oxygen reduction reaction (ORR) at the fuel cell cathode. For metal nanoparticle catalysts, proper particle dispersion, as well as good electrical contact to the working electrode are essential aspects and are generally provided by a stable, high surface area, conducting carbon support such as Vulcan XC-72.[4,5] Yet, these widely used commercial supports still suffer from purity and stability, so to remedy this, other carbonaceous support have been evaluated including mesoporous carbon,[6,7] 1D supports like carbon fibers[8,9] and nanotubes,[10,11] and graphene derivatives such as reduced graphene oxide (RGO) and graphene quantum dots (GQDs).[12−17] Of these graphitic materials, GQDs have displayed promising results as a metal nanoparticle support, a likely consequence of their natural conductivity, robustness, and high surface area.[18] Additionally, it has been found that GQDs can enhance the activity of the supported nanoparticles through manipulation of the electronic structure of the metal nanoparticles by the GQD structural defects.[16,17]

The role of the support is generally to disperse the metal nanoparticle catalysts and allow for facile charge transfer but does not impart any effects on the active metal catalyst and is therefore termed a passive support.[19] Electronic interactions between GQDs and metal nanoparticle catalysts that result in modification of the catalytic properties of the metals would render the GQDs as an active support. In the case of nanosized graphene fragments, there may be abundant oxygenated moieties on the surface depending on the synthetic routes. For instance, GQDs synthesized through chemical oxidation

Received: June 28, 2016
Revised: October 3, 2016
Published: October 11, 2016





DOI: 10.1021/acssuschemeng.6b01476
ACS Sustainable Chem. Eng. 2016, 4, 6580−6589

and exfoliation of bulk graphite typically exhibit significant oxygen content, as evidenced in XPS analysis as well as high solubility in water.[18,20−22] The oxygen groups are thought to disrupt the $sp^2$ delocalization network, resulting in a partial loss of the conductivity and diminishment of the stability, and are therefore commonly associated with defects in the graphitic backbone.[23,24] Despite these possible negative aspects, controlling the level of defects is recently gaining attention as effective avenues to the manipulation of the interactions between the GQD and the associated metal particles.[16,17,20] First of all, the oxygen groups are viewed as possible anchoring points for nanoparticle adhesion which may benefit the durability of the composites by impeding particle agglomeration during electrochemical cycling.[25] Additionally, DFT studies have proposed that the electronegative oxygen moieties will withdraw electrons from the bound metal nanoparticles, thus allowing more favorable interactions with the intermediates during oxygen reduction.[26,27]

In fact, recent experimental studies have detailed the enhancement of the ORR activity of GQD-supported platinum, palladium, and copper nanoparticles.[14−17] In these studies, the GQDs were derived from chemical exfoliation of the nanometer-sized graphitic domains in carbon pitch fibers, with a few nanometers in diameter and three to four graphene layers in thickness. The GQDs exhibited various oxygenated species and their concentrations were readily manipulated by hydrothermal treatment at controlled temperatures, as quantitatively determined by XPS and Raman measurements, and the ORR activity of the corresponding metal−GQD nanocomposites displayed a volcano-shaped variation with the GQD defect concentration. For metals like platinum, palladium, and copper that bind too tightly to oxygen, according to the so-called volcano plot,[28−35] the GQD structural defects that are electron withdrawing in nature may be exploited to lower the d band center of the associated metals, leading to weakened interactions with oxygen intermediates and hence enhanced catalytic performance. Yet, at too high defect concentrations the weakened interactions begin to hinder activity due to insufficient initial adsorption of oxygen and/or reduced electrical conductivity. This rise and fall of the ORR activity with the defect level is in strong agreement with the standing theories on the correlation between the d band structure and the strength of interactions between adsorbate and catalyst surface.[28,29,36] Experimentally, the optimal defect concentration was identified at ca. 20%, 50%, and 63% for PtGQD, PdGQD, and CuGQD,[14−17] respectively, consistent with increasing binding strength to oxygen of Pt < Pd < Cu.

While the manipulation of oxygenated defects has indeed afforded a control over the activity of the associated metal particles, the rather high levels of defects required for optimal ORR activity will likely compromise the conductivity and the eventual performance. An alternative is the incorporation of heteroatoms into the graphitic structure, in particular, nitrogen. The doping of nitrogen into the carbon backbone has been achieved by nitrogen plasma treatment of graphene nanoplatelets,[37,38] hydrothermal treatment of GQDs in ammonia,[39−41] and direct fixation from nitrogen in the air,[42] as well as by bottom-up synthesis based on CVD[43−45] or solvothermal methods utilizing nitrogen containing precursors.[46,47] Nitrogen may be incorporated into the graphitic structure as pyridinic, pyrrolic, or graphitic quaternary centers, which are easily distinguished by XPS measurements based on the different binding energies of the N 1s electrons.[38,43,47,48] Since nitrogen is more electronegative than carbon, it is likely that these centers will withdraw electron density from carbons, similar to oxygen, but without the disruption of the delocalized electron cloud since nitrogen centers are incorporated within the C $sp^2$ hybridization network. That is, nitrogen may provide the electron withdrawal necessary for activity enhancement of the metal nanoparticles but without compromising the electrical conductivity and stability of the carbon support.[14−17] These unique characteristics of nitrogen-doped GQDs (NGQDs) may be exploited to further enhance the ORR activity of palladium nanoparticles by forming PdNGQD nanocomposites. At present, palladium is less expensive and more abundant than platinum and is therefore valuable in the search for an economically viable clean energy source. Although the intrinsic catalytic activity is not generally seen as comparable to that of platinum, palladium electrocatalysts have displayed competitive activity and exhibited enhanced activity upon functionalization with N-doped graphene, but the optimization of the synthetic conditions for such a system remains largely unexplored.[49] This is the primary motivation of the present study.

Herein, a series of nanocomposites based on palladium nanoparticles supported on NGQDs were prepared by hydrothermal treatment at 160 °C of citric acid and urea in the presence of palladium(II) chloride for varied periods of time (note that prior studies based on metal-GQD nanocomposites have identified 160 °C as the optimal hydrothermal temperature[14−17]). The concurrent formation of NGQD and Pd nanoparticles allowed intimate contacts between them, as manifested in microscopic and spectroscopic measurements. Nitrogen was found to be incorporated into the graphitic structure in the p-type pyrrolic and pyridinic forms only, and their concentrations, along with the overall structural defects of the resulting NGQDS, were found to vary with the hydrothermal reaction time. The resulting nanocomposites exhibited apparent ORR activity in alkaline media, which was markedly higher than that with undoped GQDs. Control experiments with NGQDs-supported ruthenium nanoparticles prepared in a similar fashion suggested only minimal contributions from the NGQDs alone to the observed ORR activity, within the present experimental context. Significantly, a strong correlation was observed between the ORR activity and the pyrrolic nitrogen concentrations, due to the greater acidity of pyrrolic nitrogens than pyridinic ones such that more effective electron-withdrawing from the supported palladium nanoparticles.

## EXPERIMENTAL SECTION

**Chemicals.** Palladium(II) chloride ($PdCl_2$, 59% Pd, ACROS), ruthenium(III) chloride ($RuCl_3$, anhydrous 99+%, Acros), citric acid (anhydrous, 99%, Acros), urea (98%, Acros), sodium carbonate ($Na_2CO_3$, 99.5%, Fisher Scientific), hydrochloric acid (HCl, 70 wt %, ACROS), and ultrahigh-purity nitrogen and oxygen (99.993%, Praxair) were used as received. Water was supplied by a Barnstead Nanopure water system (18.3 MΩ cm).

**Nanocomposite Synthesis.** PdNGQD nanocomposites were synthesized by adopting a bottom-up procedure for NGQDs reported in the literature that involved hydrothermal treatment of citric acid and urea.[50] In a typical reaction, $PdCl_2$ (50 mg) was dissolved in 1 mL of concentrated HCl to form the water-soluble $PdCl_4^{2-}$ complex, followed by neutralization with $Na_2CO_3$, and centrifugation to remove excess salts. The palladium solution was then condensed to 2.5 mL before being added to a Teflon autoclave liner. Citric acid (70 mg) and urea (60 mg) as well as 2.5 mL of propylene glycol were also added to the liner and all the salts were allowed to dissolve. Then the solution was heated at 160 °C for various periods of time (1, 4, 8, or 12 h), resulting in the formation of large black precipitates in the bottom of


DOI: 10.1021/acssuschemeng.6b01476
ACS Sustainable Chem. Eng. 2016, 4, 6580−6589

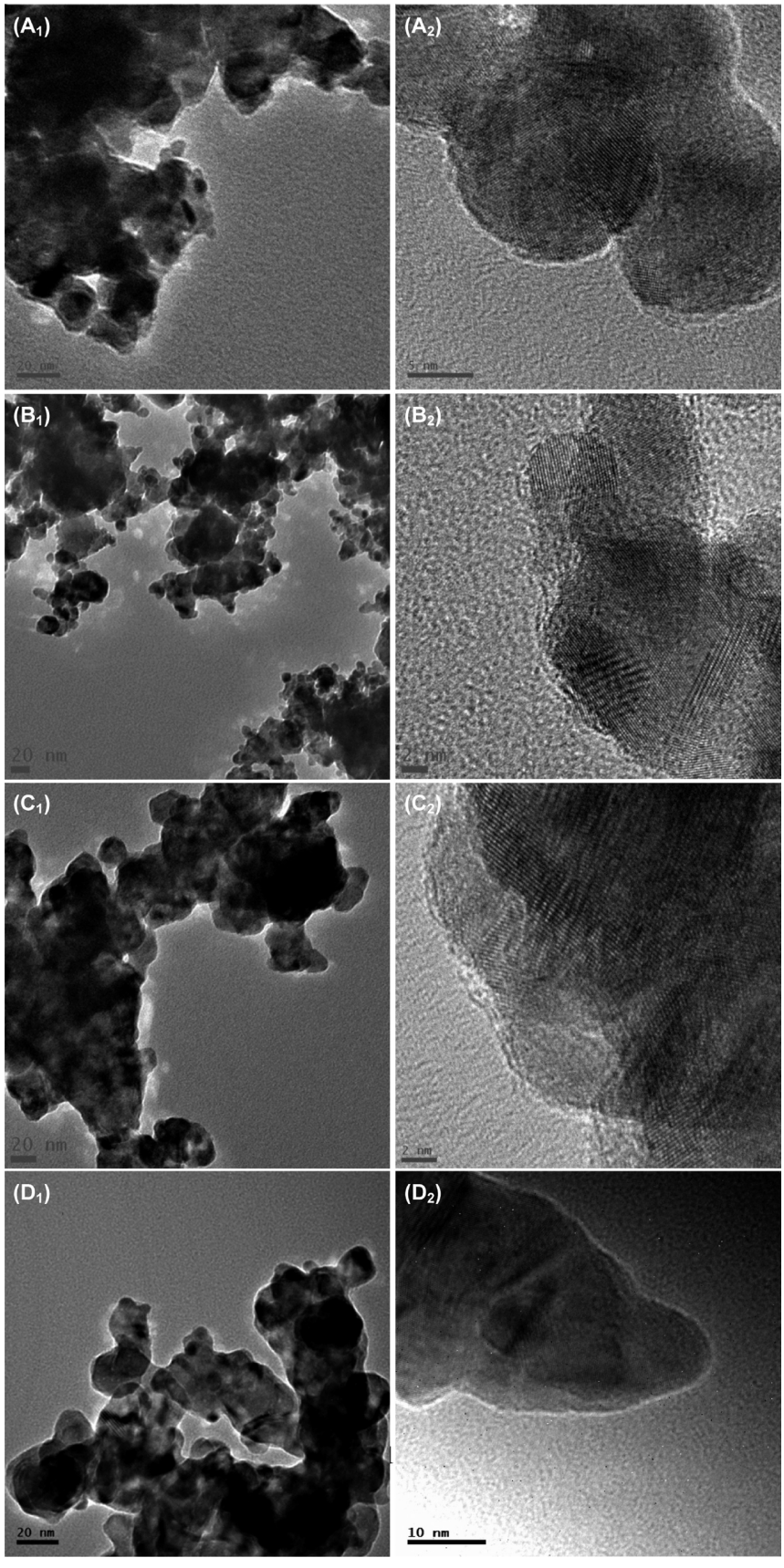


**Figure 1.** Representative TEM images of ($A_1$ and $A_2$) PdNGQD-1, ($B_1$ and $B_2$) PdNGQD-4, ($C_1$ and $C_2$) PdNGQD-8, ($D_1$ and $D_2$) PdNGQD-12. Scale bars are all 20 nm in panels $A_1$−$D_1$, 5 nm in panel $A_2$, 2 nm in $B_2$ and $C_2$, and 10 nm in $D_2$.



DOI: 10.1021/acssuschemeng.6b01476
*ACS Sustainable Chem. Eng.* 2016, 4, 6580−6589

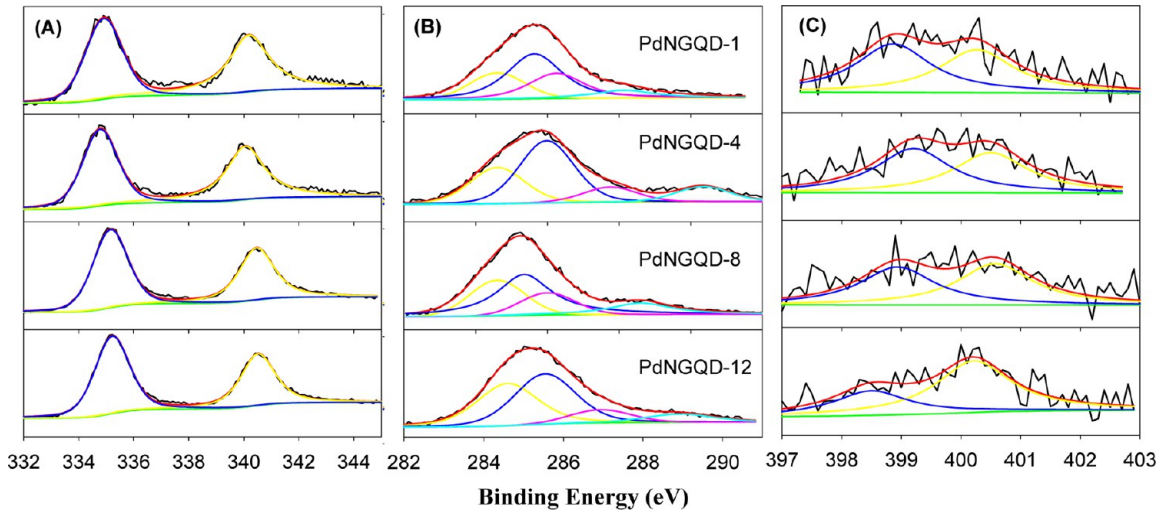


**Figure 2.** High-resolution XPS spectra of (A) Pd 3d, (B) C 1s, and (C) N 1s electrons of the series of PdNGQD nanocomposites. Black curves are experimental data and colored curves are deconvolution fits.

**Table 1. Summary of the XPS Results of the Series of PdNGQD Nanocomposites**

| | Pd | | | N dopants | | | |
|---|---|---|---|---|---|---|---|
| sample | Pd 3d5/2 (eV) | Pd 3d3/2 (eV) | Pd (at %) | pyridinic N (eV) | pyrrolic N (eV) | N (at %) | pyridinic/pyrrolic N ratio |
| PdNGQD-1 | 334.9 | 340.2 | 3.1 | 398.7 | 400.0 | 10.2 | 1.32 |
| PdNGQD-4 | 334.8 | 340.2 | 2.9 | 398.8 | 399.9 | 9.0 | 1.06 |
| PdNGQD-8 | 335.1 | 340.4 | 6.9 | 398.4 | 400.3 | 10.0 | 0.40 |
| PdNGQD-12 | 335.2 | 340.5 | 6.0 | 398.2 | 399.9 | 10.8 | 0.37 |

the liner. The precipitates were collected and purified extensively with water. The obtained samples were denoted as PdNGQD-t (with t being the heating time).

Control experiments were also carried out where a stoichiometric amount (70 mg) of $RuCl_3$ was used instead of $PdCl_2$ while keeping other experimental conditions unchanged (heating for 8 h), resulting in the formation of ruthenium nanoparticles supported on NGQD. The composite was denoted as RuNGQD. Additional controls were carried out where urea was replaced with a stoichiometric amount of citric acid, affording palladium nanoparticles supported on nitrogen-free GQDs. These samples were referred to as PdGQD-t.

**Characterizations.** Transmission electron microscopic (TEM) studies were carried out with a Philips CM300 scope (300 kV). Samples were prepared by dropcasting a dispersion of the nanocomposites prepared above in ethanol onto a carbon-coated copper grid. X-ray photoelectron spectra (XPS) were recorded with a PHI 5400/XPS instrument equipped with an Al K$\alpha$ source operated at 350 W and $10^{-9}$ Torr. Raman spectra were acquired with a Delta NU 532 nm Raman spectrometer.

**Electrochemistry.** Electrochemical tests were carried out in a standard three-electrode cell connected to a CHI 710C electrochemical workstation, with a Pt foil counter electrode and a Ag/AgCl reference electrode. The reference electrode was calibrated against a reversible hydrogen electrode (RHE) and all potentials in the present study were referred to the RHE. The working electrode was a rotating gold ring/glassy-carbon disk electrode (RRDE, from Pine Instrument, with a collection efficiency $N$ = 40%).[51] A calculated amount of the nanocomposites prepared above was dispersed in ethanol to prepare a catalyst ink, which was then slowly dropcast onto the glassy-carbon disk electrode of the RRDE and dried under gentle $N_2$. The catalyst films were then coated with 3 $\mu$L of a dilute Nafion solution (0.1 wt %) and dried in air.

## RESULTS AND DISCUSSION

NGQDs have been prepared by hydrothermal reactions of citric acid and urea at elevated temperatures (Figure S1).[50] In the present study, the addition of a controlled amount of metal salts led to in situ formation of metal nanoparticles supported on the NGQD molecular skeletons. Panels $A_1$–$D_1$ of Figure 1 depict the representative TEM micrographs of the series of PdNGQD nanocomposites. It can be seen that the composites all entailed nanoparticles of 10–20 nm clustered into larger superstructures of 100 nm and above. This morphology is similar to that of the nanocomposites where palladium was deposited onto carbon nanoparticles or GQDs derived from pitch fiber.[17,52] However, as the electron density is much lower for carbon, it is difficult to identify the carbon materials in PdNGQDs. This is very likely a result of the dynamics of simultaneous formation of NGQD and Pd nanoparticles that resulted in the embedment of metal nanostructures within the graphitic matrix.[53−55] In the high-resolution images of panels $A_2$–$D_2$, clearly defined lattice fringes can be readily observed where the interplanar spacing of 0.23 nm is consistent with that of the (111) crystalline planes of *fcc* palladium. Similar structures were observed with the PdGQD samples (Figure S2), whereas for the RuNGQD sample (Figure S3), ruthenium nanoparticles were substantially smaller with a diameter of ca. 3 nm, and the lattice fringes of 0.21 nm are in good agreement with the interplanar distance between Ru(101) crystalline planes.[56]

The formation of PdNGQD nanocomposites was confirmed by XPS measurements, where C 1s, Pd 3d, and N 1s electrons can be readily identified in the survey spectra at the binding energies of ca. 285, 340, and 400 eV, respectively (Figure S4). Further insights into the elemental compositions and valence states of the nanocomposites were obtained from the high resolution scans of the C 1s, N 1s, and Pd 3d electrons, which are depicted in Figure 2. From panel A, one can see that the PdNGQD-1 and PdNGQD-4 samples both exhibited a doublet


DOI: 10.1021/acssuschemeng.6b01476
ACS Sustainable Chem. Eng. 2016, 4, 6580−6589

at ca. 334.9 and 340.2 eV, consistent with the Pd $3d_{5/2}$ and $3d_{3/2}$ electrons of metallic palladium, respectively.[57] Yet these binding energies increased slightly with the samples prepared by longer hydrothermal reactions, 335.1 and 340.4 eV for PdNGQD-8 and 335.2 and 340.5 eV for PdNGQD-12. The results are summarized in Table 1.

For the C 1s electrons in panels B, deconvolution of the spectra yields four subpeaks, $sp^2$ carbon (C═C, yellow curves) at 284.7 eV, C−OH (dark blue curves) at 285.6 eV, carbonyl (C═O, pink curves) at 286.5 eV, and carboxylic (COOH, light blue curves) at 288.2 eV in each sample, indicating the formation of a large number of oxygenated species in the hydrothermal synthesis of NGQDs by citric acid and urea.[50] However, the concentrations of these carbon species varied markedly among the samples. In fact, based on the integrated peak areas, one can see that the fraction of (electron-withdrawing) C═O/COOH carbons decreased markedly with prolonging hydrothermal reaction time, at ca. 33% for PdNGQD-1, 30% for PdNGQD-4, 29% for PdNGQD-8, and 13% for PdNGQD-12. This may be, at least in part, ascribed to the thermal instability of the C═O/COOH moieties. In fact, in previous studies with Pt, Pd and Cu nanoparticles supported on GQDs derived from carbon pitch fiber,[14−17] it has been observed that the C═O/COOH moieties could be removed effectively by hydrothermal treatment. Further contributions may arise from interfacial decarboxylation catalyzed by Pd.[58]

In the N 1s spectra in panel (C), two major components can be identified by deconvolution. The peaks at ca. 398.5 eV (yellow curves) may be assigned to pyridinic nitrogen, whereas the other at ca. 400.0 eV (blue curve) most likely arose from pyrrolic nitrogen (Table 1).[59] This suggests that nitrogen was indeed doped into the graphitic molecular skeleton forming NGQDs. It should be noted that no quaternary nitrogen was identified at 401.7 eV. This is in sharp contrast with results observed previously in the hydrothermal synthesis of NGQDs with citric acid and urea but without the addition of metal salts, where an abundance of quaternary nitrogen was found with no signal from pyridinic nitrogen.[50] In the present study, the same procedure was adopted to prepare PdNGQD by adding a calculated amount of metal salts into the hydrothermal reactions. The fact that only p-type pyridinic and pyrrolic nitrogens were formed in the graphitic scaffolds of PdNGQD is likely due to the preferred binding of palladium to these two nitrogen moieties.

Interestingly, based on the integrated peak areas, the overall concentration of nitrogen dopants was found to be almost invariant among the series of PdNGQD at 10 at % (the corresponding concentration for Pd was 3.1 at % for PdNGQD-1, 2.9 at % for PdNGQD-4, 6.9 at % for PdNGQD-8, and 6.0 at % for PdNGQD-12, Table 1); yet, the fractions of the pyrrolic and pyridinic nitrogens varied significantly. From Figure 3A and Table 1, one can see that the pyridinic nitrogen fraction decreased markedly, whereas the fraction of the pyrrolic nitrogen increased accordingly, with prolonging hydrothermal reaction time. This implies a gradual transformation of pyridinic nitrogens into pyrrolic nitrogens during the hydrothermal synthesis. Note that in an earlier study where urea was utilized to dope graphene oxide and Pd nanoparticles were deposited on the resulting nitrogen-doped graphene oxide through thermal reduction of $Pd^{2+}$ in a water/glycol mixture at 110 °C for 7 h,[60] XPS analysis showed that pyrrolic nitrogens accounted for over 80% of the nitrogen dopants. Additionally, it has been observed that palladium

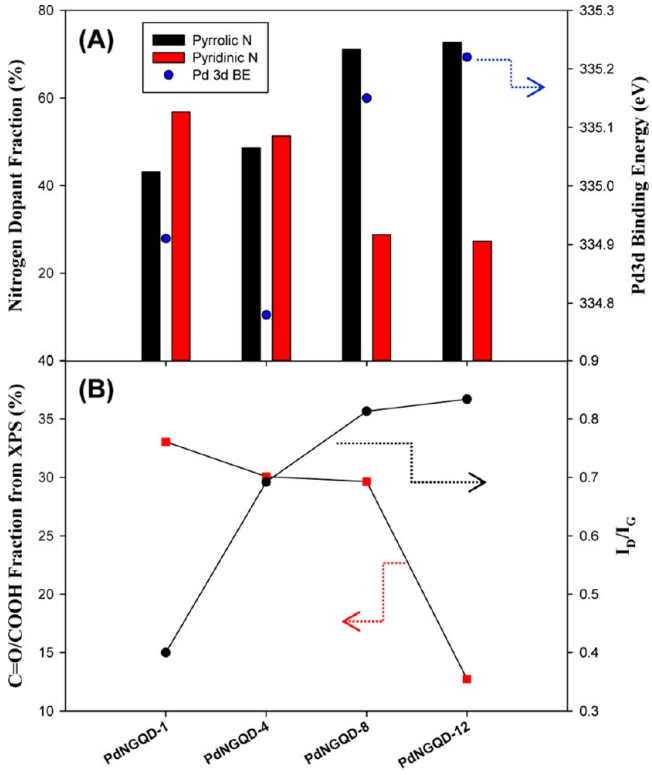


**Figure 3.** (A) Abundance of pyrrolic and pyridinic nitrogens, Pd $3d_{5/2}$ binding energy, (B) percentage of oxygenated carbon from XPS, and $I_D/I_G$ ratio from Raman measurements for the series of PdNGQD nanocomposites.

catalyzes the selective transformation of imines into pyrrolic derivatives at moderate temperatures and in the presence of oxygen.[61]

Because pyrrolic nitrogen is known to be more acidic than pyridinic nitrogen (though both are of p-type doping),[62−65] the increase of the pyrrolic nitrogen fraction would lead to a more apparent diminishment of the Pd electron density, due to the intimate interactions between palladium and the nitrogen dopants. Indeed, this is consistent with results from Figure 2A, where the Pd 3d binding energy increased from PdNGGQD-1 to PdNGQD-12, as depicted in Figure 3A and Table 1—in contrast, for PdGQD nanocomposites, prolonging hydrothermal time actually led to an decrease of the Pd 3d binding energy (Figure S5), due to diminishment of the oxygenated moieties, as observed previously.[14−17] In fact, regression analysis showed a linear fit between the abundance of pyrrolic nitrogens and the Pd 3d binding energy with an $R^2$ value of 0.83, while a negative correlation was observed for the linear fit between C═O/COOH carbon abundance and Pd 3d binding energy, with an $R^2$ value of only 0.48 (Figure S6). This strongly indicates that pyrrolic nitrogens are the primary source of electronic modulation for palladium nanoparticles, within the present experimental context. Importantly, as the relative amount of pyrrolic nitrogens is well correlated with hydrothermal reaction time, deliberate structural manipulation may be achieved. Whereas additional contributions might arise from oxygenated species as observed previously with undoped GQDs,[14−17] the present observations imply that pyrrolic nitrogen likely dominated the manipulation of the metal nanoparticle properties, as nitrogen centers act as stronger anchoring sites than oxygen moieties.


DOI: 10.1021/acssuschemeng.6b01476
ACS Sustainable Chem. Eng. 2016, 4, 6580−6589

The formation of PdNGQD nanocomposites was further confirmed by Raman spectroscopic measurements. Typically, graphitic material displays a G band (~1585 $cm^{-1}$) which represents the high frequency phonon of $E_{2g}$ symmetry within $sp^2$ carbons, as well as a D band (1350 $cm^{-1}$) which represents the phonon of $A_{1g}$ symmetry arising from a breathing mode at crystallite boundaries.[66−68] Since the G band arises from extended C $sp^2$ domains and the D band from interruptions in these domains, the relative ratio of their intensities ($I_D/I_G$) is widely used as a descriptor of the defect density for graphitic materials. Figure 4 depicts the Raman spectra of the series of

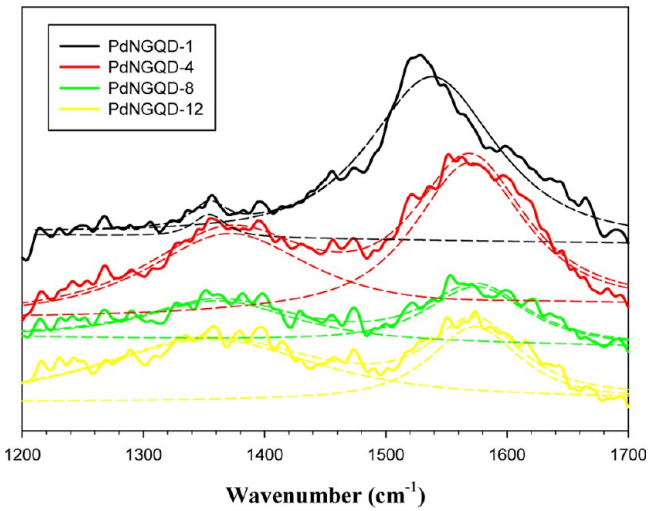


**Figure 4.** Raman spectra of PdNGQD nanocomposites. Solid curves are experimental data, and dashed curves are deconvolution fits.

the PdNGQD nanocomposites, where the D and G bands are rather well-defined for each sample, indicating the successful graphitization of citric acid and urea by hydrothermal treatments.[50] Yet marked differences can be seen upon a closer analysis. For instance, whereas the D band positions are very consistent among the samples at ca. 1360 $cm^{-1}$, the G band positions are markedly different. Specifically, the G band energy increased in the order of PdNGQD-1 (1538 $cm^{-1}$) < PdNGQD-4 (1569 $cm^{-1}$) < PdNGQD-8 ≈ PdNGQD-12 (1574 $cm^{-1}$), suggesting that prolonging hydrothermal reaction time led to shrinking C $sp^2$ domains of the resulting NGQDs. Consistent results were obtained in the comparison of the $I_D/I_G$ ratio, which increased in the same order of PdNGQD-1 (0.036) < PdNGQD-4 (0.82) < PdNGQD-8 (1.02) < PdNGQD-12 (2.06), indicating an increasingly defective structure of the NGQDs (note that the results of RuNGQD were similar to those of PdNGQD-8, Figure S7). This is in agreement with the increasing abundance of pyrrolic moieties in the series of PdNGQD samples, where the five-member pyrrolic rings would introduce enhanced geometrical strains to the graphitic matrix, as compared to the six-member pyridinic moieties. In contrast, for the control samples of PdGQDs (Figure S7), a red-shift of the G band energy, along with a decreasing $I_D/I_G$ ratio, was observed with increasing hydrothermal reaction time, indicating an increasing degree of graphitization of the GQDs due to effective removal of oxygenated species, as observed previously.[28,29,36]

Significantly, the series of PdNGQD composites all displayed apparent electrocatalytic activity toward oxygen reduction. A calculated amount of the nanocomposite catalysts was loaded onto a clean glassy carbon electrode, which was subject to electrochemical activation by rapid potential cycling within the potential range of +0.3 to +1.0 V in a nitrogen-saturated 0.1 M KOH solution. This range was deliberately chosen to avoid any complications from hydrogen absorption in Pd. From the steady-state voltammograms (Figure S8), a small broad peak between +0.65 and +0.95 V can be seen in the anodic scan, accompanied by a larger, sharper peak centered around +0.72 V in the cathodic scan. These respectively represent the formation and reduction of an oxide monolayer on the surface of the palladium particles and may be utilized to estimate the electrochemical surface area (ECSA), which is 3.80 $m^2/g_{Pd}$ for PdNGQD-1, 1.37 $m^2/g_{Pd}$ for PdNGQD-4, 2.46 $m^2/g_{Pd}$ for PdNGQD-8, and 1.98 $m^2/g_{Pd}$ for PdNGQD-12. These low values of ECSA are consistent with the rather extensive agglomeration of palladium particles observed in TEM measurements (Figure 1). Additionally, the palladium surface might be covered by NGQDs which further limited the electrochemical accessibility.

Figure 5A displays the RRDE voltammograms of the series of PdNGQD nanocomposites at the rotation rate of 1600 rpm in $O_2$-saturated 0.1 M KOH. It can be seen that for each sample, nonzero current started to occur as the potential was swept negatively past ca. +0.99 V, increased rapidly with electrode potentials, and reached a plateau at potentials more negative than around +0.70 V, indicating marked electrocatalytic activity of the PdNGQD nanocomposites toward oxygen reduction. Yet, from the voltammograms, one can see that the ORR activity varied among the series of PdNGQD nanocomposites. For instance, at +0.70 V, the current density increased by the following order, PdNGQD-1 (40.8 $A/m^2$) < PdNGQD-4 (51.8 $A/m^2$) < PdNGQD-8 (61.6 $A/m^2$) ≈ PdNGQD-12 (61.8 $A/m^2$), indicating that samples synthesized by longer hydrothermal reactions exhibited much better ORR activity. A similar trend can also be observed by comparing the mass activity, 24.9 $A/g_{Pd}$ for PdNGQD-4 < 33.4 $A/g_{Pd}$ for PdNGQD-12 < 56.0 $A/g_{Pd}$ for PdNGQD-8 < 63.2 $A/g_{Pd}$ for PdNGQD-1. The fact that the mass activity of PdNGQD-1 was the highest among the series was most likely due to the good dispersion and surface accessibility of the Pd nanoparticles, as manifested in the quantification of ECSA (Figure S8).

In addition, by setting the ring potential at +1.5 V, collection experiments showed that the ring currents were at least 2 orders of magnitude lower than the disk currents (more in Figure S9), suggesting the production of only a minimal amount of peroxide species during oxygen reduction. In fact, using the data in panel (A) as the example, the number of electron transfer ($n$) during ORR was evaluated with the equation, $n = \frac{4I_{disk}}{I_{disk} + \frac{I_{ring}}{N}}$, where $I_{disk}$ and $I_{ring}$ are the voltammetric currents at the disk and ring electrode respectively, and N is the collection efficiency (40%).[51] From panel (B), one can see that for the PdNGQD-8 sample, $n$ is almost 4 within a wide potential range of +0.50 to +1.0 V, indicating that oxygen underwent complete (4e) reduction to $OH^-$, $O_2 + 2H_2O + 4e \rightarrow 4OH^-$. The PdNGQD-1 sample also showed $n \approx 4$, but only at potentials less positive than +0.90, whereas for PdNGQD-4 and PdNGQD-12, the electrode potential must be even more negative than +0.85 V. Taken together, these results indicate that the PdNGQD-8 sample stood out as the best catalyst among the series toward ORR.

Consistent behaviors were observed in the Tafel plot, where the kinetic current density was quantitatively assessed by


DOI: 10.1021/acssuschemeng.6b01476
ACS Sustainable Chem. Eng. 2016, 4, 6580−6589

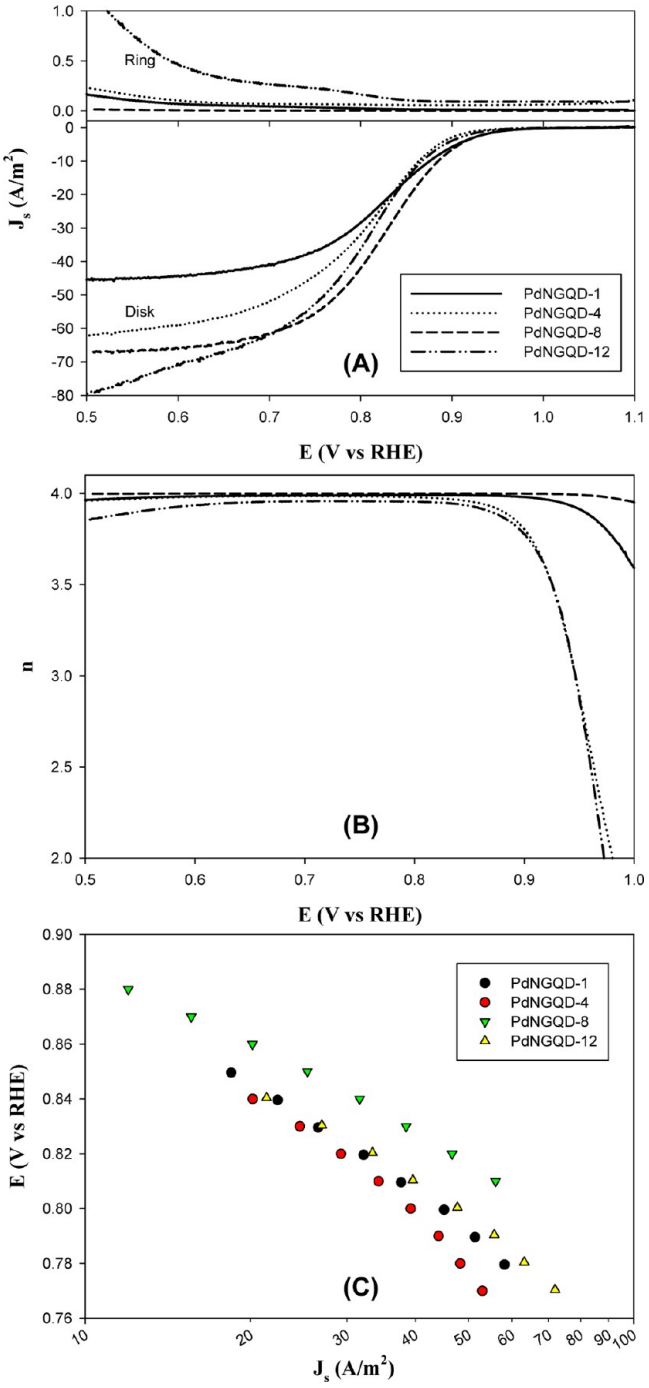


**Figure 5.** (A) RRDE voltammograms of the series of PdNGQD nanocomposites in oxygen-saturated 0.1 M KOH at the electrode rotation rate of 1600 rpm. The potential of the ring electrode is set at +1.5 V. The palladium loadings are 6.52 $\mu$g for PdNGQD-1, 7.82 $\mu$g of Pd for PdNGQD-4, 6.28 $\mu$g for PdNGQD-8, and 5.01 $\mu$g for PdNGQD-12. DC ramp 10 mV/s. (B) Variation of the number of electron transfer ($n$) with electrode potentials. Data are calculated from the RRDE voltammograms in panel A. (C) Tafel plots of the PdNGQD nanocomposites. Data are obtained from the Koutecky–Levich plots in Figure S10. Current density is calculated by normalizing the voltammetric current to the respective electrochemical surface area estimated from Figure S8 based on the reduction of palladium oxide.

Koutecky–Levich (KL) analysis (Figure S10). From panel (C), it can be seen that for the PdNGQD series, the kinetic current density all increased drastically with increasingly negative electrode potential, due to enhanced electron transfer kinetics in ORR, and the Tafel slopes were found to be very close, at 138 mV/dec for PdNGQD-1, 138 mV/dec for PdNGQD-4, 120 mV/dec for PdNGQD-8, and 128 mV/dec for PdNGQD-12, suggesting a similar reaction mechanism for ORR where the first electron reduction of oxygen was likely the rate-determining step.[69] In addition, it can also be seen that at all potentials the PdNGQD-8 sample exhibited the highest specific activity among the series of samples. For example, at +0.85 V, the specific current density was around 18.8 A/m$^2$ for PdNGQD-1, PdNGQD-4, and PdNGQD-12 but increased by about 35% to 25.4 A/m$^2$ for PdNGQD-8. This is likely a result of the strong influence by the nitrogen centers that facilitated charge transfer and provided optimal binding interactions between the metal surface and oxygenated intermediates.

Recently it has been shown that nitrogen-doped graphene derivatives exhibit high electrocatalytic activity toward ORR, which is largely attributed to carbons bonded to pyridinic or graphitic nitrogens.[70] In the present study, whereas pyridinic nitrogens were also formed in the PdNGQD nanocomposites, control experiments with RuNGQDs showed minimal contributions from the NGQDs to the ORR activity. As seen from Figure S11, the onset potential for RuNGQD was around +0.70 V, about 300 mV more negative than that for any of the PdNGQD composites (Figure 5A). Also, the RuNGQD did not really reach a current plateau even at potentials more negative than +0.50 V and the current density was markedly lower. These results indicate that, in the present study, the ORR activity was primarily attributed to Pd in the hybrids, not the nitrogen dopants. Furthermore, the specific activity of PdNGQD-8 was over 8 times better than results of the PdGQD nanocomposites (where oxygenated moieties were presumed to be the major structural defects responsible for the manipulation of the ORR activity)[17] and commercial Pt/C.[14] This may be ascribed to the incorporation of pyridinic and pyrrolic nitrogens into the graphitic skeletons, as both are of p-type doping[62−65] that would further modulate the electron density of the palladium nanoparticles and hence the bonding interactions with oxygen intermeidates.[14−17] In addition, the fact that the ORR activity increased with increasing abundance of pyrrolic nitrogens in the series of PdNGQD (Figure 5) may be accounted for by the higher acidity of pyrrolic nitrogen than pyridinic nitrogen.[71,72] This observation is also consistent with results from XPS measurements (Figure 3). Certainly, at too high pyrrolic contents, the electronic conductivity of the nanocomposites may be compromised due to the enhanced geometrical strains and structural defects. Therefore, within the present experimental context, the PdNGQD-8 sample represented an optimal composition for ORR among the series.

Notably, the activity of the PdNGQD nanocomposites observed above compared very well to those of relevant composites based on palladium nanoparticles supported on graphitic substrates. For example, palladium nanoparticles of 2.3 and 3.3 nm in diameter have been deposited on Vulcan XC72 carbon by chemical and thermal reduction of an organometallic precursor,[73] and the resulting hybrids displayed an onset potential for ORR that was more than 100 mV more negative than the results observed above for the PdNGQD series (Figure 5). In another study,[74] RGO-supported palladium nanoparticles (average diameter 3 nm) were prepared by photoassisted reduction of $Na_2PdCl_4$ and displayed a mass activity of 88 A/$g_{Pd}$ at +0.765 V vs RHE in oxygen-


DOI: 10.1021/acssuschemeng.6b01476
ACS Sustainable Chem. Eng. 2016, 4, 6580−6589

saturated 0.1 M KOH. In the present study, the palladium nanoparticles were all markedly larger (aggregates >100 nm); yet the activity remained highly comparable. This, again, strongly suggests that deliberate incorporation of selected nitrogen dopants may be exploited for drastic enhancements of the nanocomposite ORR activity.

## CONCLUSION

In this study, PdNGQD nanocomposites were synthesized by hydrothermal coreduction of palladium salt, citric acid, and urea at 160 °C for varied periods of time (1, 4, 8, or 12 h), leading to intimate contact between the metal nanostructures and nitrogen-doped graphitic backbone. TEM studies revealed rather extensive aggregation of palladium nanoparticles in PdNGQDs. XPS measurements showed that nitrogen was indeed doped into the graphitic molecular skeleton in the forms of p-type pyrrolic and pyridinic nitrogens only; and whereas the total concentration of the nitrogen dopants was rather consistent among the series of samples, the relative abundance of pyrrolic (pyridinic) N actually increased (decreased) with prolonging hydrothermal time. The binding energy of the Pd 3d electrons was found to increase concurrently, which might be accounted for by the greater acidity (electron-withdrawing) of pyrrolic nitrogen than pyridinic nitrogen. Consistent results were obtained in Raman measurements, which suggested increasingly defective structures of the graphitic skeletons due to the increasing concentration of five-member pyrrolic rings. Significantly, the PdNGQD nanocomposites all showed apparent ORR activity in alkaline media, and PdNGQD-8 was found to exhibit the best specific activity among the series, which was over 8 times better than that of the PdGQD counterparts and commercial Pt/C. This suggests an optimal degree of electron withdrawal from the metal cores by the acidic pyrrolic N (p-type) dopants that were more effective in modulating the electron density of the supported palladium nanoparticles than oxygenated moieties alone in undoped GQDs. Furthermore, control experiments with RuNGQD suggested minimal contributions from the NGQDs to the ORR activity, within the present experimental context. As the type of nitrogen dopants may be readily manipulated by experimental conditions, the results herein suggest an easy, energy-efficient method for the synthesis of effective ORR catalysts based on heteroatom-doped GQD-supported metal nanoparticles.

## ASSOCIATED CONTENT

### Supporting Information

The Supporting Information is available free of charge on the ACS Publications website at DOI: 10.1021/acssuschemeng.6b01476.

Additional experimental results including TEM, XPS, Raman, and voltammetric data (PDF)

## AUTHOR INFORMATION

### Corresponding Author

*E-mail: shaowei@ucsc.edu.

### Notes

The authors declare no competing financial interest.

## ACKNOWLEDGMENTS

This work was supported, in part, by grants from the National Science Foundation (CHE-1265635 and DMR-1409396). TEM and XPS work was carried out at the National Center for Electron Microscopy and Molecular Foundry at the Lawrence Berkeley National Laboratory, as part of a user project, which is supported by the U.S. Department of Energy.

## REFERENCES

(1) Cano-Castillo, U. Hydrogen and Fuel Cells: Potential Elements in the Energy Transition Scenario. *Rev. Mex Fis* **2013**, *59*, 85−92.
(2) Hamrock, S. J.; Herring, A. M.; Zawodzinski, T. A. Fuel cell chemistry and operation. *J. Power Sources* **2007**, *172*, 1−1.
(3) Dhathathreyan, K. S.; Sridhar, P.; Sasikumar, G.; Ghosh, K. K.; Velayutham, G.; Rajalakshmi, N.; Subramaniam, C. K.; Raja, M.; K, R. Development of polymer electrolyte membrane fuel cell stack. *Int. J. Hydrogen Energy* **1999**, *24*, 1107−1115.
(4) Sharma, S.; Pollet, B. G. Support materials for PEMFC and DMFC electrocatalysts-A review. *J. Power Sources* **2012**, *208*, 96−119.
(5) Zhou, X. J.; Qiao, J. L.; Yang, L.; Zhang, J. J. A Review of Graphene-Based Nanostructural Materials for Both Catalyst Supports and Metal-Free Catalysts in PEM Fuel Cell Oxygen Reduction Reactions. *Adv. Energy Mater.* **2014**, *4*, 1301523.
(6) Ding, J.; Chan, K. Y.; Ren, J. W.; Xiao, F. S. Platinum and platinum-ruthenium nanoparticles supported on ordered mesoporous carbon and their electrocatalytic performance for fuel cell reactions. *Electrochim. Acta* **2005**, *50*, 3131−3141.
(7) Joo, S. H.; Kwon, K.; You, D. J.; Pak, C.; Chang, H.; Kim, J. M. Preparation of high loading Pt nanoparticles on ordered mesoporous carbon with a controlled Pt size and its effects on oxygen reduction and methanol oxidation reactions. *Electrochim. Acta* **2009**, *54*, 5746−5753.
(8) Ledesma-García, J.; Escalante García, I. L.; Rodríguez, F. J.; Chapman, T. W.; Godínez, L. A. Immobilization of dendrimer-encapsulated platinum nanoparticles on pretreated carbon-fiber surfaces and their application for oxygen reduction. *J. Appl. Electrochem.* **2008**, *38*, 515−522.
(9) Hsin, Y. L.; Hwang, K. C.; Yeh, C. T. Poly(vinylpyrrolidone)-modified graphite carbon nanofibers as promising supports for PtRu catalysts in direct methanol fuel cells. *J. Am. Chem. Soc.* **2007**, *129*, 9999−10010.
(10) Kongkanand, A.; Kuwabata, S.; Girishkumar, G.; Kamat, P. Single-wall carbon nanotubes supported platinum nanoparticles with improved electrocatalytic activity for oxygen reduction reaction. *Langmuir* **2006**, *22*, 2392−2396.
(11) Yoon, B.; Wai, C. M. Microemulsion-templated synthesis of carbon nanotube-supported pd and rh nanoparticles for catalytic applications. *J. Am. Chem. Soc.* **2005**, *127*, 17174−17175.
(12) Li, Y.; Li, Y.; Zhu, E.; McLouth, T.; Chiu, C.-Y.; Huang, X.; Huang, Y. Stabilization of High-Performance Oxygen Reduction Reaction Pt Electrocatalyst Supported on Reduced Graphene Oxide/Carbon Black Composite. *J. Am. Chem. Soc.* **2012**, *134*, 12326−12329.
(13) Lim, E. J.; Choi, S. M.; Seo, M. H.; Kim, Y.; Lee, S.; Kim, W. B. Highly dispersed Ag nanoparticles on nanosheets of reduced graphene oxide for oxygen reduction reaction in alkaline media. *Electrochem. Commun.* **2013**, *28*, 100−103.
(14) He, G. Q.; Song, Y.; Liu, K.; Walter, A.; Chen, S.; Chen, S. W. Oxygen Reduction Catalyzed by Platinum Nanoparticles Supported on Graphene Quantum Dots. *ACS Catal.* **2013**, *3*, 831−838.
(15) Liu, K.; Song, Y.; Chen, S. W. Oxygen reduction catalyzed by nanocomposites based on graphene quantum dots-supported copper nanoparticles. *Int. J. Hydrogen Energy* **2016**, *41*, 1559−1567.
(16) Song, Y.; Chen, S. W. Graphene Quantum-Dot-Supported Platinum Nanoparticles: Defect-Mediated Electrocatalytic Activity in Oxygen Reduction. *ACS Appl. Mater. Interfaces* **2014**, *6*, 14050−14060.
(17) Deming, C. P.; Mercado, R.; Gadiraju, V.; Sweeney, S. W.; Khan, M.; Chen, S. Graphene Quantum Dots-Supported Palladium Nanoparticles for Efficient Electrocatalytic Reduction of Oxygen in Alkaline Media. *ACS Sustainable Chem. Eng.* **2015**, *3*, 3315−3323.
(18) Peng, J.; Gao, W.; Gupta, B. K.; Liu, Z.; Romero-Aburto, R.; Ge, L.; Song, L.; Alemany, L. B.; Zhan, X.; Gao, G.; Vithayathil, S. A.;



DOI: 10.1021/acssuschemeng.6b01476
*ACS Sustainable Chem. Eng.* 2016, 4, 6580−6589

Kaipparettu, B. A.; Marti, A. A.; Hayashi, T.; Zhu, J. J.; Ajayan, P. M. Graphene quantum dots derived from carbon fibers. *Nano Lett.* **2012**, *12*, 844−849.
(19) Hu, P. G.; Liu, K.; Deming, C. P.; Chen, S. W. Multifunctional graphene-based nanostructures for efficient electrocatalytic reduction of oxygen. *J. Chem. Technol. Biotechnol.* **2015**, *90*, 2132−2151.
(20) He, D. P.; Cheng, K.; Peng, T.; Sun, X. L.; Pan, M.; Mu, S. C. Bifunctional effect of reduced graphene oxides to support active metal nanoparticles for oxygen reduction reaction and stability. *J. Mater. Chem.* **2012**, *22*, 21298−21304.
(21) Bacon, M.; Bradley, S. J.; Nann, T. Graphene Quantum Dots. *Part Part Syst. Char* **2014**, *31*, 415−428.
(22) Stankovich, S.; Dikin, D. A.; Piner, R. D.; Kohlhaas, K. A.; Kleinhammes, A.; Jia, Y.; Wu, Y.; Nguyen, S. T.; Ruoff, R. S. Synthesis of graphene-based nanosheets via chemical reduction of exfoliated graphite oxide. *Carbon* **2007**, *45*, 1558−1565.
(23) Wang, J. J.; Yin, G. P.; Shao, Y. Y.; Wang, Z. B.; Gao, Y. Z. Investigation of further improvement of platinum catalyst durability with highly graphitized carbon nanotubes support. *J. Phys. Chem. C* **2008**, *112*, 5784−5789.
(24) Li, L.; Xing, Y. C. Electrochemical durability of carbon nanotubes in noncatalyzed and catalyzed oxidations. *J. Electrochem. Soc.* **2006**, *153*, A1823−A1828.
(25) Hull, R. V.; Li, L.; Xing, Y. C.; Chusuei, C. C. Pt nanoparticle binding on functionalized multiwalled carbon nanotubes. *Chem. Mater.* **2006**, *18*, 1780−1788.
(26) Lim, D. H.; Wilcox, J. Mechanisms of the Oxygen Reduction Reaction on Defective Graphene-Supported Pt Nanoparticles from First-Principles. *J. Phys. Chem. C* **2012**, *116*, 3653−3660.
(27) Liu, X.; Li, L.; Meng, C.; Han, Y. Palladium Nanoparticles/Defective Graphene Composites as Oxygen Reduction Electrocatalysts: A First-Principles Study. *J. Phys. Chem. C* **2012**, *116*, 2710−2719.
(28) Stephens, I. E. L.; Bondarenko, A. S.; Grønbjerg, U.; Rossmeisl, J.; Chorkendorff, I. Understanding the electrocatalysis of oxygen reduction on platinum and its alloys. *Energy Environ. Sci.* **2012**, *5*, 6744.
(29) Kitchin, J. R.; Norskov, J. K.; Barteau, M. A.; Chen, J. G. Modification of the surface electronic and chemical properties of Pt(111) by subsurface 3d transition metals. *J. Chem. Phys.* **2004**, *120*, 10240−10246.
(30) Lima, F. H. B.; Zhang, J.; Shao, M. H.; Sasaki, K.; Vukmirovic, M. B.; Ticianelli, E. A.; Adzic, R. R. Catalytic Activity-d-Band Center Correlation for the O2 Reduction Reaction on Platinum in Alkaline Solutions. *J. Phys. Chem. C* **2007**, *111*, 404−410.
(31) Hammer, B.; Norskov, J. K. Electronic factors determining the reactivity of metal surfaces. *Surf. Sci.* **1995**, *343*, 211−220.
(32) Hennig, D.; GandugliaPirovano, M. V.; Scheffler, M. Adlayer core-level shifts of admetal monolayers on transition-metal substrates and their relation to the surface chemical reactivity. *Phys. Rev. B: Condens. Matter Mater. Phys.* **1996**, *53*, 10344−10347.
(33) Bzowski, A.; Sham, T. K.; Watson, R. E.; Weinert, M. Electronic-Structure of Au and Ag Overlayers on Ru(001) - the Behavior of the Noble-Metal D-Bands. *Phys. Rev. B: Condens. Matter Mater. Phys.* **1995**, *51*, 9979−9984.
(34) Weinert, M.; Watson, R. E. Core-Level Shifts in Bulk Alloys and Surface Adlayers. *Phys. Rev. B: Condens. Matter Mater. Phys.* **1995**, *51*, 17168−17180.
(35) Toyoda, E.; Jinnouchi, R.; Hatanaka, T.; Morimoto, Y.; Mitsuhara, K.; Visikovskiy, A.; Kido, Y. The d-Band Structure of Pt Nanoclusters Correlated with the Catalytic Activity for an Oxygen Reduction Reaction. *J. Phys. Chem. C* **2011**, *115*, 21236−21240.
(36) Norskov, J. K.; Rossmeisl, J.; Logadottir, A.; Lindqvist, L.; Kitchin, J. R.; Bligaard, T.; Jonsson, H. Origin of the Overpotential for Oxygen Reduction at a Fuel-Cell Cathode. *J. Phys. Chem. B* **2004**, *108*, 17886−17892.
(37) Jafri, R. I.; Rajalakshmi, N.; Ramaprabhu, S. Nitrogen doped graphene nanoplatelets as catalyst support for oxygen reduction reaction in proton exchange membrane fuel cell. *J. Mater. Chem.* **2010**, *20*, 7114−7117.
(38) Chetty, R.; Kundu, S.; Xia, W.; Bron, M.; Schuhmann, W.; Chirila, V.; Brandl, W.; Reinecke, T.; Muhler, M. PtRu nanoparticles supported on nitrogen-doped multiwalled carbon nanotubes as catalyst for methanol electrooxidation. *Electrochim. Acta* **2009**, *54*, 4208−4215.
(39) Sun, H. J.; Gao, N.; Wu, L.; Ren, J. S.; Wei, W. L.; Qu, X. G. Highly Photoluminescent Amino-Functionalized Graphene Quantum Dots Used for Sensing Copper Ions. *Chem. - Eur. J.* **2013**, *19*, 13362−13368.
(40) Hu, C. F.; Liu, Y. L.; Yang, Y. H.; Cui, J. H.; Huang, Z. R.; Wang, Y. L.; Yang, L. F.; Wang, H. B.; Xiao, Y.; Rong, J. H. One-step preparation of nitrogen-doped graphene quantum dots from oxidized debris of graphene oxide. *J. Mater. Chem. B* **2013**, *1*, 39−42.
(41) Tian, R. X.; Hu, S. L.; Wu, L. L.; Chang, Q.; Yang, J. L.; Liu, J. Tailoring surface groups of carbon quantum dots to improve photoluminescence behaviors. *Appl. Surf. Sci.* **2014**, *301*, 156−160.
(42) Jeon, I. Y.; Choi, H. J.; Ju, M. J.; Choi, I. T.; Lim, K.; Ko, J.; Kim, H. K.; Kim, J. C.; Lee, J. J.; Shin, D.; Jung, S. M.; Seo, J. M.; Kim, M. J.; Park, N.; Dai, L.; Baek, J. B. Direct nitrogen fixation at the edges of graphene nanoplatelets as efficient electrocatalysts for energy conversion. *Sci. Rep.* **2013**, *3*, 2260.
(43) Jin, Z.; Yao, J.; Kittrell, C.; Tour, J. M. Large-Scale Growth and Characterizations of Nitrogen-Doped Monolayer Graphene Sheets. *ACS Nano* **2011**, *5*, 4112−4117.
(44) Koos, A. A.; Murdock, A. T.; Nemes-Incze, P.; Nicholls, R. J.; Pollard, A. J.; Spencer, S. J.; Shard, A. G.; Roy, D.; Biro, L. P.; Grobert, N. Effects of temperature and ammonia flow rate on the chemical vapour deposition growth of nitrogen-doped graphene. *Phys. Chem. Chem. Phys.* **2014**, *16*, 19446−19452.
(45) Wei, D. C.; Liu, Y. Q.; Wang, Y.; Zhang, H. L.; Huang, L. P.; Yu, G. Synthesis of N-Doped Graphene by Chemical Vapor Deposition and Its Electrical Properties. *Nano Lett.* **2009**, *9*, 1752−1758.
(46) Deng, D.; Pan, X.; Yu, L.; Cui, Y.; Jiang, Y.; Qi, J.; Li, W.-X.; Fu, Q.; Ma, X.; Xue, Q.; Sun, G.; Bao, X. Toward N-Doped Graphene via Solvothermal Synthesis. *Chem. Mater.* **2011**, *23*, 1188−1193.
(47) Li, Y.; Zhao, Y.; Cheng, H.; Hu, Y.; Shi, G.; Dai, L.; Qu, L. Nitrogen-doped graphene quantum dots with oxygen-rich functional groups. *J. Am. Chem. Soc.* **2012**, *134*, 15−18.
(48) Wang, G.; Jia, L. T.; Zhu, Y.; Hou, B.; Li, D. B.; Sun, Y. H. Novel preparation of nitrogen-doped graphene in various forms with aqueous ammonia under mild conditions. *RSC Adv.* **2012**, *2*, 11249−11252.
(49) Jukk, K.; Kongi, N.; Matisen, L.; Kallio, T.; Kontturi, K.; Tammeveski, K. Electroreduction of oxygen on palladium nanoparticles supported on nitrogen-doped graphene nanosheets. *Electrochim. Acta* **2014**, *137*, 206−212.
(50) Qu, D.; Zheng, M.; Du, P.; Zhou, Y.; Zhang, L.; Li, D.; Tan, H.; Zhao, Z.; Xie, Z.; Sun, Z. Highly luminescent S, N co-doped graphene quantum dots with broad visible absorption bands for visible light photocatalysts. *Nanoscale* **2013**, *5*, 12272−12277.
(51) Zhou, Z. Y.; Kang, X. W.; Song, Y.; Chen, S. W. Enhancement of the electrocatalytic activity of Pt nanoparticles in oxygen reduction by chlorophenyl functionalization. *Chem. Commun.* **2012**, *48*, 3391−3393.
(52) Huang, J.; Zhou, Z.; Song, Y.; Kang, X. W.; Liu, K.; Zhou, W.; Chen, S. W. Electrocatalytic Activity of Palladium Nanocatalysts Supported on Carbon Nanoparticles in Formic Acid Oxidation. *J. Electrochem* **2012**, *18*, 508−514.
(53) Templeton, A. C.; Wuelfing, M. P.; Murray, R. W. Monolayer protected cluster molecules. *Acc. Chem. Res.* **2000**, *33*, 27−36.
(54) Chen, S. W.; Templeton, A. C.; Murray, R. W. Monolayer-protected cluster growth dynamics. *Langmuir* **2000**, *16*, 3543−3548.
(55) Lim, B.; Jiang, M. J.; Camargo, P. H. C.; Cho, E. C.; Tao, J.; Lu, X. M.; Zhu, Y. M.; Xia, Y. N. Pd-Pt Bimetallic Nanodendrites with High Activity for Oxygen Reduction. *Science* **2009**, *324*, 1302−1305.
(56) Ghosh, D.; Chen, S. W. Solid-state electronic conductivity of ruthenium nanoparticles passivated by metal-carbon covalent bonds. *Chem. Phys. Lett.* **2008**, *465*, 115−119.
(57) Wagner, C. D.; Riggs, W. M.; Davis, L. E.; Moulder, J. F.; Muilenberg, G. E. *Handbook of x-ray photoelectron spectroscopy: a*


DOI: 10.1021/acssuschemeng.6b01476
*ACS Sustainable Chem. Eng.* 2016, 4, 6580−6589

*reference book of standard data for use in x-ray photoelectron spectroscopy*; Perkin-Elmer Corp.: Eden Prairie, MN, 1979.
(58) Chen, L. M.; Song, Y.; Hu, P. G.; Deming, C. P.; Guo, Y.; Chen, S. W. Interfacial reactivity of ruthenium nanoparticles protected by ferrocenecarboxylates. *Phys. Chem. Chem. Phys.* **2014**, *16*, 18736−18742.
(59) Liu, X. J.; Li, L. G.; Zhou, W. J.; Zhou, Y. C.; Niu, W. H.; Chen, S. W. High-Performance Electrocatalysts for Oxygen Reduction Based on Nitrogen-Doped Porous Carbon from Hydrothermal Treatment of Glucose and Dicyandiamide. *ChemElectroChem* **2015**, *2*, 803−810.
(60) Movahed, S. K.; Dabiri, M.; Bazgir, A. Palladium nanoparticle decorated high nitrogen-doped graphene with high catalytic activity for Suzuki-Miyaura and Ullmann-type coupling reactions in aqueous media. *Appl. Catal., A* **2014**, *488*, 265−274.
(61) Meng, L.; Wu, K.; Liu, C.; Lei, A. Palladium-catalysed aerobic oxidative Heck-type alkenylation of Csp3-H for pyrrole synthesis. *Chem. Commun.* **2013**, *49*, 5853−5855.
(62) Schiros, T.; Nordlund, D.; Palova, L.; Prezzi, D.; Zhao, L. Y.; Kim, K. S.; Wurstbauer, U.; Gutierrez, C.; Delongchamp, D.; Jaye, C.; Fischer, D.; Ogasawara, H.; Pettersson, L. G. M.; Reichman, D. R.; Kim, P.; Hybertsen, M. S.; Pasupathy, A. N. Connecting Dopant Bond Type with Electronic Structure in N-Doped Graphene. *Nano Lett.* **2012**, *12*, 4025−4031.
(63) Fujimoto, Y.; Saito, S. Formation, stabilities, and electronic properties of nitrogen defects in graphene. *Phys. Rev. B: Condens. Matter Mater. Phys.* **2011**, *84*, 245446.
(64) Hou, Z. F.; Wang, X. L.; Ikeda, T.; Terakura, K.; Oshima, M.; Kakimoto, M. Electronic structure of N-doped graphene with native point defects. *Phys. Rev. B: Condens. Matter Mater. Phys.* **2013**, *87*, 165401.
(65) Kim, H. S.; Kim, H. S.; Kim, S. S.; Kim, Y. H. Atomistic mechanisms of codoping-induced p- to n-type conversion in nitrogen-doped graphene. *Nanoscale* **2014**, *6*, 14911−14918.
(66) Dresselhaus, M. S.; Terrones, M. Carbon-Based Nanomaterials From a Historical Perspective. *Proc. IEEE* **2013**, *101*, 1522−1535.
(67) Ferrari, A. C.; Basko, D. M. Raman spectroscopy as a versatile tool for studying the properties of graphene. *Nat. Nanotechnol.* **2013**, *8*, 235−246.
(68) Tuinstra, F. Raman Spectrum of Graphite. *J. Chem. Phys.* **1970**, *53*, 1126−1130.
(69) Song, C. J.; Zhang, J. J. Electrocatalytic Oxygen Reduction Reaction. In *PEM Fuel Cell Electrocatalysis and Catalyst Layers: Fundamentals and Applications*; Zhang, J. L., Ed.; Springer, 2008; pp 89−134.
(70) Guo, D. H.; Shibuya, R.; Akiba, C.; Saji, S.; Kondo, T.; Nakamura, J. Active sites of nitrogen-doped carbon materials for oxygen reduction reaction clarified using model catalysts. *Science* **2016**, *351*, 361−365.
(71) Kang, H. S.; Jeong, S. Nitrogen doping and chirality of carbon nanotubes. *Phys. Rev. B: Condens. Matter Mater. Phys.* **2004**, *70*, 233411.
(72) Ewels, C. P.; Glerup, M. Nitrogen doping in carbon nanotubes. *J. Nanosci. Nanotechnol.* **2005**, *5*, 1345−1363.
(73) Arroyo-Ramirez, L.; Montano-Serrano, R.; Luna-Pineda, T.; Roman, F. R.; Raptis, R. G.; Cabrera, C. R. Synthesis and characterization of palladium and palladium-cobalt nanoparticles on Vulcan XC-72R for the oxygen reduction reaction. *ACS Appl. Mater. Interfaces* **2013**, *5*, 11603−11612.
(74) Huang, Y. X.; Xie, J. F.; Zhang, X.; Xiong, L.; Yu, H. Q. Reduced graphene oxide supported palladium nanoparticles via photoassisted citrate reduction for enhanced electrocatalytic activities. *ACS Appl. Mater. Interfaces* **2014**, *6*, 15795−15801.


DOI: 10.1021/acssuschemeng.6b01476
*ACS Sustainable Chem. Eng.* 2016, 4, 6580−6589